Composite Structures 260 (2021) 113473

Contents lists available at ScienceDirect

Composite Structures

journal homepage: www.elsevier.com/locate/compstruct

Dynamic performance of concrete columns retrofitted with FRP using segment pressure technique

M. Abedini [a], Chunwei Zhang [a,*]

[a] School of Civil Engineering, Qingdao University of Technology, Qingdao 266033, China

ARTICLE INFO

Keywords:
RC column
Fibre Reinforced Polymer (FRP)
P-I diagram
Blast load
LS-DYNA

ABSTRACT

For RC columns exposed to blast loads, fibre reinforced polymer (FRP) is employed to examine its effectiveness in strengthening the concrete structure against blast load. It should be noted that no systematic studies could be found in the literature to derive pressure and impulse (P-I) diagram for FRP retrofitted RC columns. Therefore, the objective of this research is to develop finite element model to provide data for use in the development of P-I diagram that can be used to mitigate blast hazards and predict damage in RC columns retrofitted with FRP. In this study, various strengthening scheme performed against blast loads numerically by running computer simulations using the commercial software LS-DYNA. Validation of the models is performed based on the blast field test to investigate the accuracy of model simulations to present the behaviour of the models. The research compared the structural behaviour of an un-strengthened RC column with various column strengthened with different FRP wrap thickness, strength and arrangement. The results of the simulations showed that strengthening with FRP is an effective way to increase the blast resistance capacity of columns. This information would allow the designer to identify the critical location for placing blast barriers for protection purpose.

1. Introduction

One of the basic needs for human beings is to be secured and protected against any expected threat which can cause them any damage, especially harms threatening their lives. This started in early ages by building civilian structures which insure safety at first, and extended to include other aspects such as economy. Hence, engineers and scientists have continuously developed technologies in order to fulfill this need. From all threats, explosion is one of the most serious hazards that may arise, as many incidents have proved that it can cause economic and life losses, in addition to the associated psychological impact on the general public [1]. Structural resistance of blast loads has drawn much attention that has led to developing many guidelines to evaluate the structural performance [2–4]. As an example, a blast load destroyed three of four columns of a federal building in Oklahoma City. Sadly, the building collapsed, and many citizens injured. However, limited understanding of structural behavior subjected to extremely dynamic and short-period loads has remained problematic. Researchers then focused more on the resistance of RC columns under blast loads [5–8].

Reinforced concrete (RC) columns are crucial parts of structures as they withstand the greatest amount of structural loads. RC columns are not generally used to design to sustain extreme dynamic loads. Thus, it is necessary making RC columns highly susceptible to terrorist attacks [9]. For this reason, retrofitting methods have developed over the years from blast hardening by the addition of mass using concrete or steel, to the application of lighter and more resilient materials. Traditional retrofit methods, that use materials such as concrete or steel are difficult to construct, expensive, time consuming and can often add to the debris hazard [10]. To be useful, retrofit techniques should be able to adapt to a variety of existing conditions, be aesthetically pleasing, easily transportable and cost-effective while providing adequate blast resistance. Recently, for RC columns exposed to blast loads, fibre reinforced polymer is employed to examine in respect of its effectiveness in strengthening the concrete structure against blast load [11,12].

P–I diagrams are simplified methods that describes the response of structures to blast loads [13,14]. These diagrams determine the level of damage to buildings and can be used to estimate human response to shock waves. Current design codes recommend preparing P-I curves for real analysis of structures and human safety. P–I diagrams can be developed through field tests and analytical and numerical studies. However, blast field tests are very expensive, and the analytical methods only represent global failure. Numerical methods are generally better approaches to obtain fairly accurate structural responses.

* Corresponding author.
E-mail address: zhangchunwei@qut.edu.cn (C. Zhang).

https://doi.org/10.1016/j.compstruct.2020.113473
Received 5 June 2020; Revised 8 October 2020; Accepted 14 December 2020
Available online 23 December 2020

Various damage circumstances have been offered in P-I diagrams. In general, two separate regions are used: (1) minor damage located below the curve; (2) major damage above the curve. P–I diagrams may be divided into three different categories (see Fig. 1). P-I diagrams provide better discrimination against the quasi-static and impulse regions. The impulse asymptote is tangent to the impulsive loading region, and the pressure asymptote is tangent to the quasi-static loading region (see Fig. 1). The points on the curve denote the likelihood of any failure. Points located on the left and below the curve represent no failure in the structure. In contrast, points located above and on the right side of the plot indicate that the structure is subjected to fail.

Researchers have studied P–I diagrams to assess structural responses under blasts [15–21]. P–I diagram based on the residual capacity of columns against explosive pressures are developed in [22,23]. The effect of loading shape using P–I diagram is studied in [24] and found that the load shape factor affects the elastic range for P–I curve. P-I curve according to the extreme displacement is presented in [25]. P-I points lying on the left and below the curves indicated response levels smaller than maximum displacement. Whereas, points lying above and to the right in P-I diagrams resulted in a greater level of response than the limit.

In this study, finite element models are developed for construct pressure and impulse asymptotes to predict the behavior of un-retrofitted and retrofitted RC columns when subjected to explosion loads. In order to investigate the behaviour of the FRP strengthened RC column, three-dimensional finite element models have been developed using LS-DYNA. Validation study is performed based on the blast field test to investigate the accuracy of FE models to present the behaviour of the models. In the current research, simplified methodology is generated for applying blast loads to columns in finite element models. A parametric study will be carried out to estimate P_0 and I_0 in the reinforced concrete columns retrofitted with FRP composites when exposed to blast detonations.

2. Fibre reinforced polymer (FRP) composite

Fibre reinforced composites consist of high-strength fibres embedded in a resin matrix and when retrofitted to a column can enhance the column's blast resistance. The material properties of the composite depend on the type of fibres and resin used. Various different types of fibres can be used including glass fibres, carbon fibres, Kevlar fibres and others, all of which are available in various grades and types. Glass fibres are the most commonly used reinforcing fibre in industry due to their high strength and relatively low cost, and so are investigated in this research.

The tensile strength of FRP is approximately twice that of pre-stressed steel strands, though the FRP does not exhibit any yielding before reaching its ultimate tensile strength. The mass density of FRP is approximately four times less than that of steel. The Young's modulus of FRP is generally lower than steel, though sometimes it can be greater. The stress–strain behaviour of FRP can be considered to be linear. A composite's elongation is typically linear up to a fracture at 1% to 2% elongation. A typical tensile stress–strain curve of FRP composites is presented in Fig. 2 that indicates FRP responds linear-elastically to axial stress.

The way in which a FRP responds to axial compression depends on the volume of fibres, fibre properties, resin properties and interface bond strength. Fibre composites are anisotropic. They have high strength along the fibre length but are much weaker across the fibre axis. Table 1 shows the material properties of various FRP composites [26,27]. It can be seen that the tensile strength in the transverse direction is very poor [28].

3. Blast response of un-retrofitted and FRP retrofitted columns

3.1. Experimental blast field test

Baylot and Benvis (2007) investigated the response of five scaled two-story RC frames against nearby blast fields. The Baylot and Benvis' second experiment is used to validate the current study by simulating the behavior of the middle column (see Fig. 3). The charge is considered hemispherical C4 placed in opposition to the central column served as the test column. Baylot and Benvis reported experimental and numerical techniques including detail structural configuration, test observations, material data, geometries, and blast parameters. Average values used in the test are listed in Table 2. Explosive mass is 7.087Kg C4 with 1.07 m as standoff distance from the middle column and 0.2286 m from the ground.

The strengthening of RC column subjected to blast loading retrofitted with FRP have been carried out by Crawford et al. [30]. They generated a baseline design for a multistory building as shown in Fig. 4. Case two of Crawford' experiment is used to validate the current study by simulating the behavior of the middle column. The FRP jackets with six layers and thickness of 0.5 mm are applied to RC column with 750 mm width, 750 mm depth and 3650 mm height. The thickness of FRP is 0.5 mm with strength and stiffness of 372 MPa and 52 GPa respectively. Eigth longitudinal rebars of $\phi = 32$ mm and transverse reinforcement of $\phi = 10$ mm with 450 mm centre to centre are included in the RC column. A blast of 683 kg is used at a standoff distance of 6.1 m. Table 3 present the properties of material applied in [30].

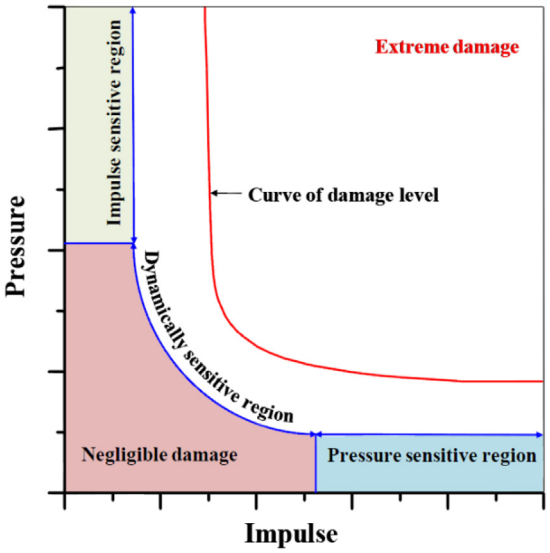

Fig. 1. Characteristic of P-I diagram.

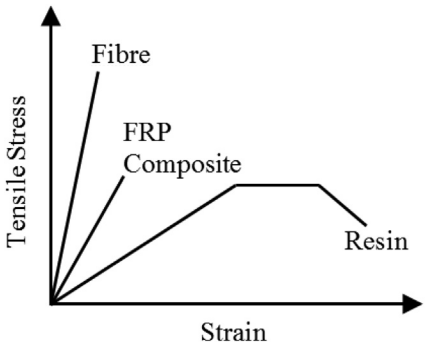

Fig. 2. Reinforced polymer stress strain graph.

Table 1
Epoxy and fibre composite properties [26–28]

Material	Density ρ (kg/m^3)	Young's modulus E (GPa)	Shear modulus G (GPa)	Ultimate Tensile strength (GPa)	Failure strain (%)	Poisson's ratio ν	Ultimate shear strength (MPa)	Ultimate compressive strength (MPa)
E-glass & epoxy (along fibre)	1800	39.3	4.8	965	5	0.3	83	620
E-glass & epoxy (across fibre)	1800	4.8	–	96.5	5	0.3	–	–
Carbon & epoxy (along fibre)	1550	137.8	5.7	1550	1.4	0.25	60	1172
Carbon & epoxy (across fibre)	1550	9	–	86.2	–	0.25	–	–
Kevlar49 & epoxy (along fibre)	1380	75.8	2.1	1378	3.1	0.34	60	276
Kevlar49 & epoxy (across fibre)	1380	5.5	–	28.3	3.1	0.34	–	–

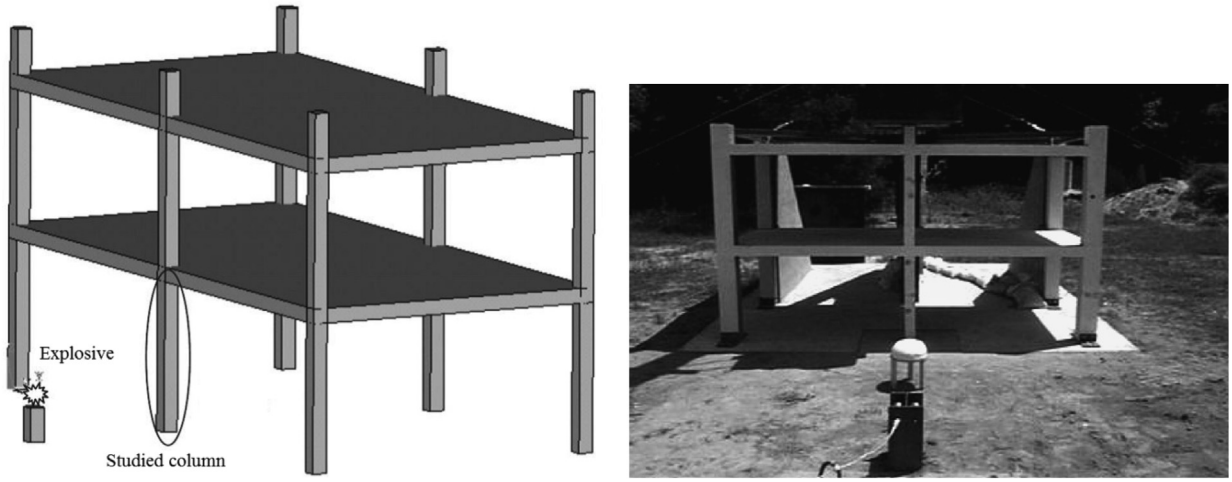

Fig. 3. Experimental model developed by Baylot and Benvis [29].

Table 2
Average value of materials used in [29].

Material	Material Properties	Values
Concrete	Concrete strength	42 MPa
Longitudinal reinforcement	Yield stress	450 MPa
	Ultimate stress	510 MPa
	Fracture strain	18%
Transverse reinforcement	Yield stress	400 MPa
	Ultimate stress	610 MPa
	Fracture strain	18%

3.2. Finite element modelling of experimental test

At first finite element modeling of experimental test performed by Baylot and Bevins presented. Schematic modeling of the FE model is presented in Fig. 5. The column cross section and height are $85 \times 85mm^2$and 0.935 mm, respectively. Eigth longitudinal rebars of $\phi = 7.1mm$ and with a transverse reinforcement of $\phi = 3.5mm$ with the cover of 8.5 mm are included in the RC column. Uniform hexahedral mesh with the size of 8.5 mm and constant stress fromulation (ELFORM = 1) and beam elements with Hughes-Liu are used for the model. Hourglass control keyword is also used during the simulation to prevent zero energy modes.

In the validation model, the head and foot of the column are fixed to inhibit translation and rotation. Top nodes, however, are free along the column axis to allow axial loads. The length of the support is 85 mm on each end at the bottom face, and hence the effective column length is considered as 935 mm between the centerline of supports. A pressure of 2.1 MPa is applied on the top surface of the column via a ramp function to consider the gravitation load before the blast simulation. Applying pressure on the front surface of the RC column with the ramp function reduces the stress concentration [31].

In this part, finite element modeling of experimental test performed by Crawford et al. is presented. The finite element model of RC column is considered with dimensions of 750 mm × 750 mm and the height is set to 3650 mm. All longitudinal reinforcement bars have cross-section with a diameter of 32 mm. The stirrups diameter is 10 mm with a spacing of 450 mm (see Fig. 6 for description). The element type and material model for steel and concrete are same with the above model. The mesh size of 50.0 mm is used for all element types. A 50 mm cover space between concrete and steel rebar is assumed for all the models studied. The Belytschko-Tsay shell element with mesh size of 50 mm × 50 mm with 0.5 mm thickness is used to model the FRP composites in LS-DYNA and the outer nodes of the FRP composites are fixed in both translation and rotation. Static axial load is applied on the head of the column to simulate static loadings of the column before the blast pressure is applied on the column surface facing the explosion center.

3.3. Blast-pressure time history representation

LSDYNA provides different approach to simulate the explosive loads in the structures [32,33]. One of the easiest methods to simulate blast load in RC structures is segment pressure time history (simplified) technique. Explosives materials are typically not modeled in this

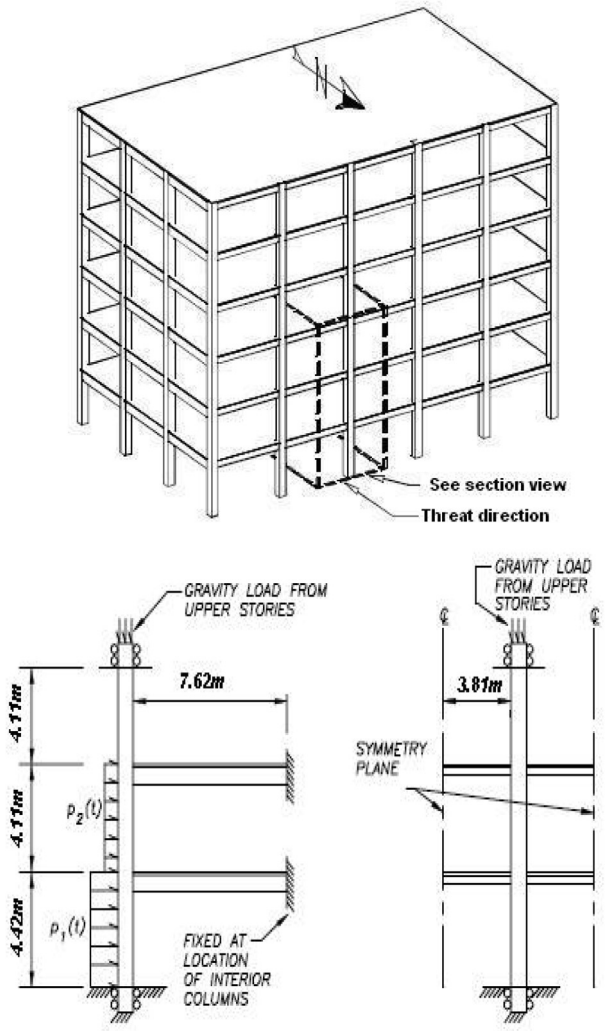

Fig. 4. Sketch of multi-story building used to calibrate the numerical model of FRP retrofitted column [30].

Table 3
Average values of materials used in [30].

Material	Parameters	Values
Concrete	strength	34.5 MPa
	Mass density	2400 kg/m^3
	Poisson's ratio	0.2
	modulus of elasticity	29 GPa
Steel Reinforcement	Young's Modulus	200 GPa
	Yield stress	414 MPa
	Mass density	7850 kg/m^3
	Poisson's ratio	0.3
	Plastic strain at failure	0.13

fashion due to the difficulties involved in obtaining the proper blast-pressure time history as the input to the problem at hand. However, in some cases, the direct pressure history approach can be advantageous in terms of run time improvements, especially for sequential blasting with multiple small charges (i.e., charges that occupy very small space relative to the total volume of the material modeled). When small charges are used in a sequential blast simulation, charges in the model that have not yet been detonated must be included in the computation of the controlling time step size. In the simplified method, the blast pressure–time history is applied as an idealized triangular ramped loading as presented in Fig. 7. Using simplified method apply a specific pressure on a surface of the Lagrangian solid. In this method, model requires a surface segment that will experience the blast loading. The load curve as seen in Fig. 13 is then used uniformly over the column front face. The Load_Segment_Set keyword in LS-DYNA is applied to describe the load curve and column surface interaction. The pressure vs. time co-ordinates is defined using Define_Curve while the surface is defined using the Set_Segment keywords. By applying triangular blast pressure to the surface of the column, the displacement time histories are obtained. In the current research, the blast loads are applied uniformly along the height of the targeted column.

3.4. Material models

The LS-DYNA software program is used extensively in research projects to simulate the blast loading of structures and the structural response [34]. To model a RC column component accurately, the materials within it must be modeled correctly. The structural failure and response of the column are highly sensitive to the material model. Furthermore, the material models available in LS-DYNA material library are applied to simulate the concrete, longitudinal reinforcement steel, stirrup steel, air and explosive.

3.4.1. Concrete material model

Concrete is the most difficult material to model because of its complex behavior under different loading situations. The Material Model 72Rel3 in LS-DYNA developed by Karagozian & Case consulting engineering firm, is chosen due to its capability of reproducing the performance of concrete exposed to different extreme events [35]. Literature has shown that material model 72Rel3 can successfully incorporate nonlinear concrete properties [36–38]. This material model is the most reliable model applied for the analysis of response under blast load and has been proven to yield more accurate results than other material models [39]. Generally, concrete failure boundaries are defined as a region created by two surfaces namely the yield surface and the maximum failure surface in a three-dimensional principal-stress space as displayed in Fig. 8. From this figure, it can be seen that the maximum failure surface and yield surface are located in the principal stress space separated at some distance away from each other. Based on the findings from previous researchers, three failure modes can be identified when the concrete's loading surface intercepts the failure surface [40]. The three failure modes are cracking, crushing and their combined effects.

For isotropic materials, like concrete, state of stress invariant functions is commonly used to develop the failure criterion and in this present study the concrete material failure criterion is defined by the stress invariants. With the stress tensor, σ_{ij}, the basic component of stress invariant functions is defined as the summation of two components namely deviatoric stress tensor,s_{ij} and hydrostatic stress tensor, $\sigma_h\delta_{ij}$. The general expression of σ_{ij} is as follows:

$$\sigma_{ij} = s_{ij} + \sigma_h\delta_{ij} \tag{1}$$

and the pure hydrostatic stress is of the form

$$\sigma_h = \frac{1}{3}(\sigma_x + \sigma_y + \sigma_z) \tag{2}$$

where σ_x, σ_y and σ_z are the principal stresses in x, y and z direction, respectively. By rearranging Eq. (1), the deviatoric stress, or the pure shear state equivalent, can then be calculated using the expression.

$$s_{ij} = \sigma_{ij} - \sigma_h\delta_{ij} \tag{3}$$

KCC model uses three shear failure surfaces namely an initial yield surface, a maximum failure surface and a residual surface with consideration of all three stress invariants as shown in Fig. 9.

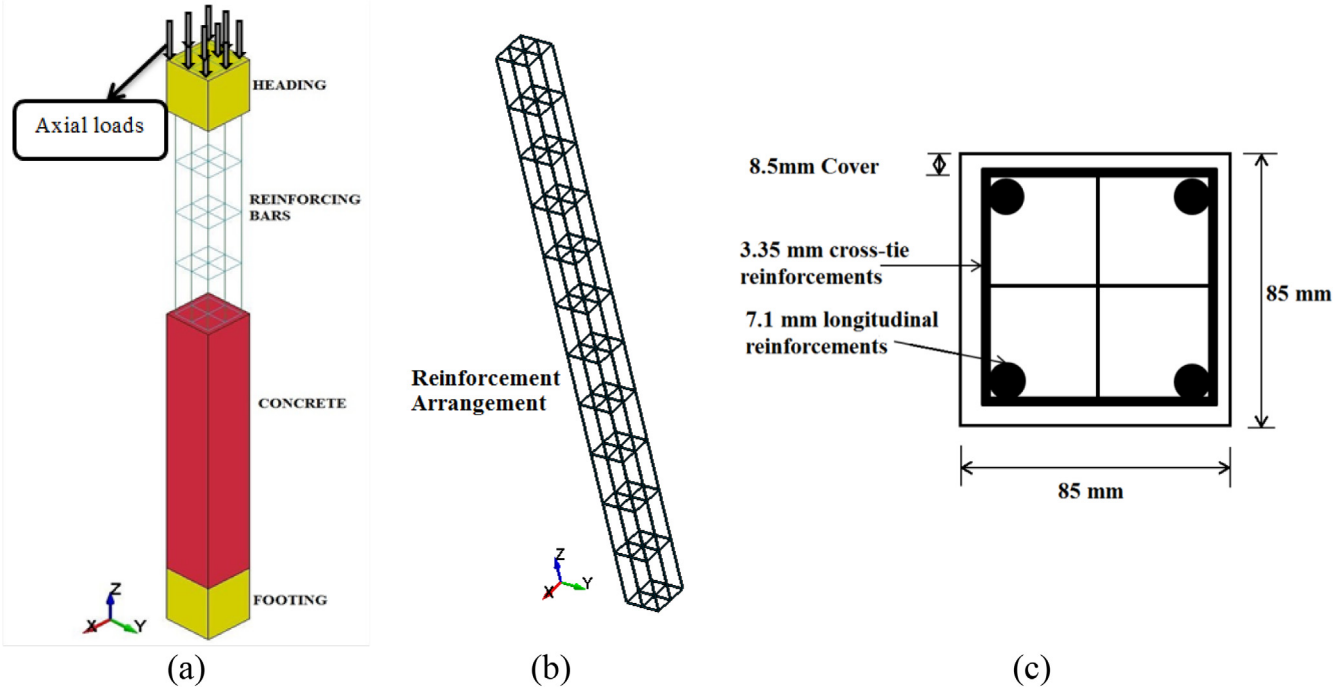

Fig. 5. (a) Details of un-strengthened RC column, (b) Reinforcement arrangement and (c) Cross section of RC column.

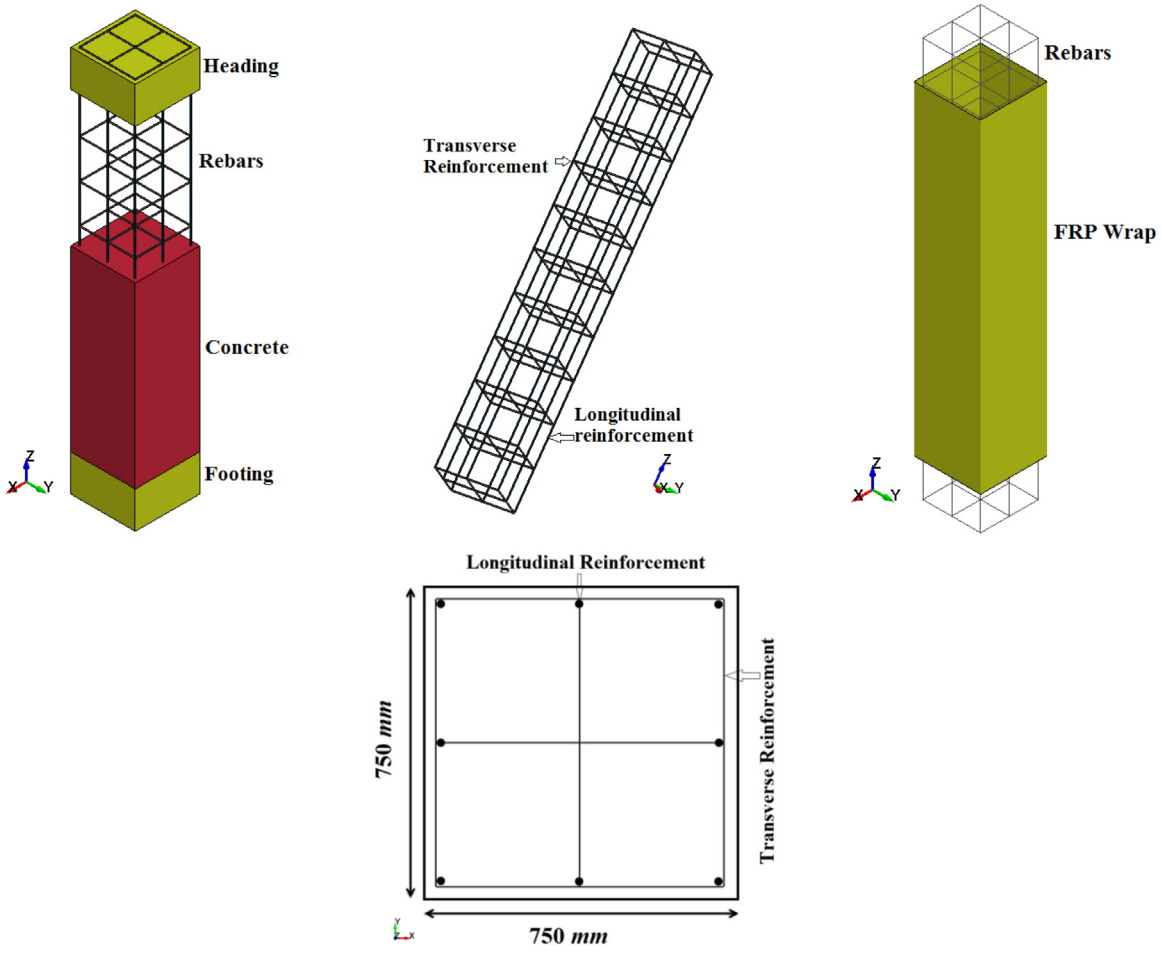

Fig. 6. Details of strengthened RC column.

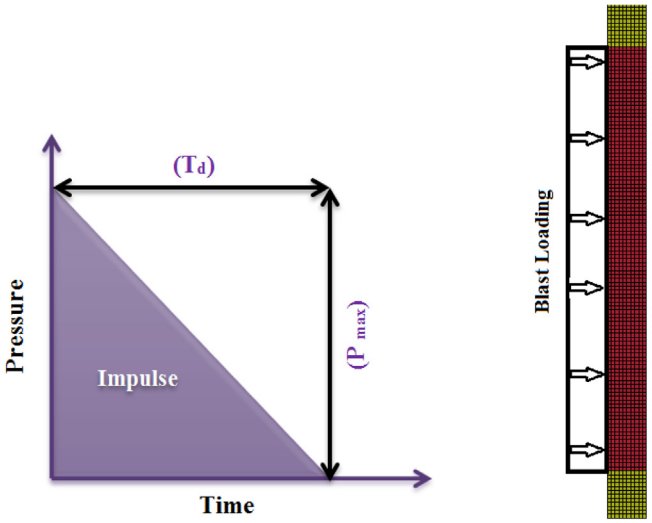

Fig. 7. Simplified blast pressure–time method.

This material model offers an added advantage of only one user input parameter; i.e. Unconfined compressive strength is sufficient in the calibration process [42,43]. Since the unconfined compressive strength of concrete can be easily determined from experimental testing, it is very useful in blast and impact simulation process. The material model charactristic in the current research is presented in Table 4.

3.4.2. Steel material model

Steel is critical components of RC structures under sever dynamic loads. Material Type 024 (Piecewise Linear Plasticity) is used to model both longitudinal and transverse steel reinforcement [44]. The Mat Piecewise Linear Plasticity is another type of a simple input model, which is exists in the LS-DYNA library. The Mat Piecewise Linear Plasticity with properties listed in Table 5 is considered for reinforcement bars [45].

3.4.3. FRP material model

In order to analyze how the FRP material will respond to blast load, a material model must be utilized and the input parameters established. The method will be used for analyses in the software LS-DYNA. The material parameters are sought primarily by testing, however in order to make the method complete literature studies have

Table 4
Material model charactristic for concrete.

MAT_CONCRETE_DAMAGE_REL3		
mass density ρ (kg/m^3)	concrete strength f_c (MPa)	Poisson's ratio υ
2400	42	0.2

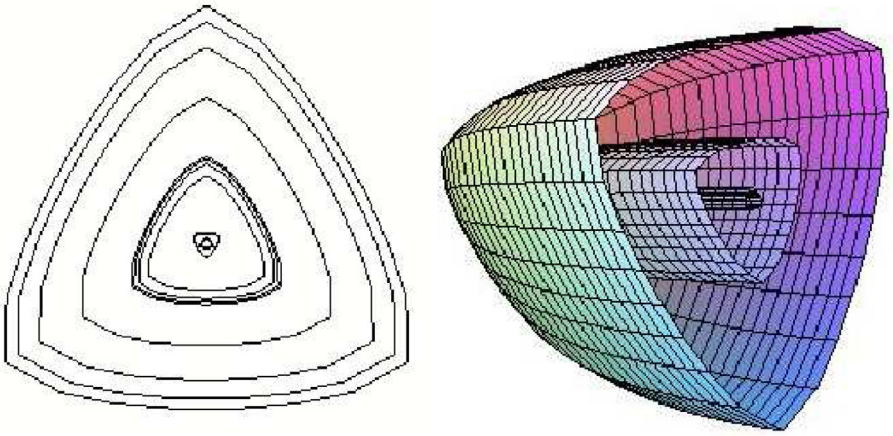

Fig. 8. Failure surfaces in 3D stress space [41].

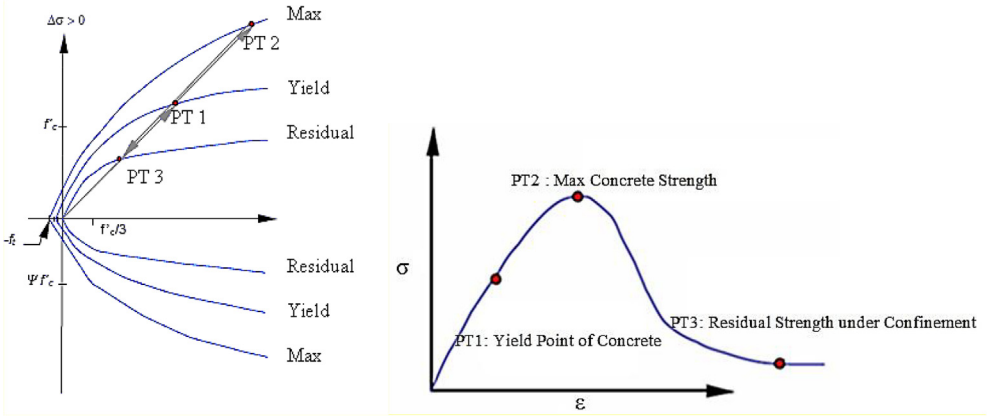

Fig. 9. Failure surfaces in Mat_Comcrete_Damage_REL3.

Table 5
Steel material properties.

mass density ρ (kg/m^3)	Young's Modulus E (GPa)	υ	longitudinal steel strength, fy (MPa)	transverse steel strength, fyt (MPa)
7800	200	0.3	450	400

been made and also reversed engineering has been used. If an appropriate material model can be combined with accurate material data realistic results can be achieved and great resources can be saved that otherwise would have been used on impact testing.

In the current research, Material Type 58 (Mat_Laminated_Composite_Fabric) in LS-DYNA is used to model the FRP material properties. It is particularly appropriate for simulating the FRP sheet for strengthening under dynamic loads. The properties of the FRP that are input into the material model are from Chan et al. [46] research work and presented in Table 6.

3.5. Strain rate effects

For the past decades, considerable effort had been made to assessment the effects of strain rate on construction materials under different loading. Steels and concretes are more resistant to high-rate dynamic loads. Blast-resistant design manual introduced Dynamic Increase Factor (DIF) which considers rate effects for the component strength [47]. DIF is a function of concrete strength at low and high strain rates [48]. For the past decades, many researchers have drawn attention to evaluating strain rate effects on construction materials under different loading. The ability of concrete to intensify at higher strain rates can be referred to DIF. Granville [49] showed the concrete compressive strength could be amplified according to the loading speed. DIFs for the compression (CDIF) and tension (TDIF) are estimated in the CEB-FIB model code as follows [50]:

$$CDIF = \frac{f_c}{f_{cs}} = \begin{cases} \left[\frac{\dot{\varepsilon}}{\dot{\varepsilon}_{cs}}\right]^{1.026\alpha} & for \quad \dot{\varepsilon} \leqslant 30\ s^{-1} \\ \gamma\left(\frac{\dot{\varepsilon}}{\dot{\varepsilon}_{cs}}\right)^{\frac{1}{3}} & for \quad \dot{\varepsilon} > 30\ s^{-1} \end{cases}$$

$$TDIF = \frac{f_t}{f_{ts}} = \begin{cases} \left[\frac{\dot{\varepsilon}}{\dot{\varepsilon}_{ts}}\right]^{\delta} & for \quad \dot{\varepsilon} \leqslant 1\ s^{-1} \\ \left[\frac{\dot{\varepsilon}}{\dot{\varepsilon}_{ts}}\right]^{\frac{1}{3}} & for \quad \dot{\varepsilon} > 1\ s^{-1} \end{cases}$$

$$log\gamma = 6.156\alpha - 0.49$$

$$\beta = 7.11\delta - 2.33$$

$$\alpha = (5 + 0.75 f_{cu})^{-1}$$

$$\delta = \left(10 + 6 f'_c / f'_{co}\right)^{-1}$$

where;

Compressive strength	**Tensile strength**
f_{cd} = dynamic compressive strength at $\dot{\varepsilon}$	f_{td} = dynamic tensile strength at $\dot{\varepsilon}$
f_c = static compressive strength at $\dot{\varepsilon}_{cs}$	f_{ts} = static tensile strength at $\dot{\varepsilon}_{ts}$
$\frac{f_{cd}}{f_c}$ = compressive strength DIF	f_{td}/f_{ts} = tensile strength DIF
f_{cu} =static cube strength = 1.205 × f_c	$\dot{\varepsilon}$ = strain rate in the range of 10^{-5} to 160 s^{-1}
$\dot{\varepsilon}_{cs}$ = 30 × 10^{-6} s^{-1} (static strain rate)	$\dot{\varepsilon}_{ts}$ = 3 × 10^{-6} s^{-1} (static strain rate)
$\dot{\varepsilon}$ = strain rate in the range of 1 to 300 s^{-1}	f'_{co} = 10 *MPa*

Steel is strain rate sensitive. Strain rates reflect in load–deflection curves of material tested under compression tests using various strain rates [51]. Malvar proposed an equation for steel rebars manufactured under ASTM standards [52]. Based on the data from the average strain rates, empirical relationship for determining the DIF of steel is derived as follows:

$$DIF = \frac{(\dot{\varepsilon})^{\alpha}}{10^{-4}} \tag{5}$$

where;

$\alpha = 0.019 - 0.009\frac{f_y}{414}$ forultimatestress
$\alpha = 0.074 - 0.040\frac{f_y}{414}$ foryieldstress
f_y = steel yield strength
$\dot{\varepsilon}$ = strain rate in the range of 0 to 225 s^{-1}

Table 6
Properties of FRP material [46].

Mechanical properties	Carbon/epoxy (AS4/3501–6)	
Density (kg/m$^{3)}$	ρ	1580
Longitudinal modulus (GPa)	E_1	138
Transverse modulus (GPa)	E_2	9.65
In-plane shear modulus	G_{21}	5.24
Out-of-plane shear modulus	G_{23}	2.24
Minor Poisson's ratio	ν_{21}	0.021
Through thickness Poisson' ratio	ν_{31}	0.021
Longitudinal tensile strength (MPa)	X_T	2280
Longitudinal compressive strength (MPa)	X_C	1440
Transverse tensile strength (MPa)	Y_T	57
Transverse compressive strength (MPa)	Y_C	228
In-plane shear strength (MPa)	S	71
Maximum strain for fibre tension (%)	ε_t	1.38
Maximum strain for fibre compression (%)	ε_c	1.175

3.6. Contact method for numerical simulations

The interaction between longitudinal rebar and concrete is essential in the dynamic simulation since the stresses flow between materials affect the dynamic response of the structure. Perfect bond assumption between concrete and reinforcement bars may not lead to reliable prediction of RC column response when the structure is subjected to the impact load [53]. Shi et al., [53] used contact function Contact-1D to model the bond slip between concrete and reinforcement bars. In the current research, the interface between steel and concrete is modeled using the one-dimensional (1D) contact formulation. With this one-dimensional slide line contact type, steel nodes as slave nodes are dependent on concrete nodes as master nodes. When parts of common shared nodes are eroded from the simulation due to material failure, contacts between structural components need to be defined; otherwise, contacting parts that are not defined may intrude into the adjoining structural components without any counterforce. Parameters to define contact-1D are presented in Table 7. In that study, the bond between the rebar and the concrete is assumed to have an elastic–plastic relation with the maximum shear stress τ_{max}. τ_{max} is calculated by

$$\tau_{max} = G_s u_{max} e^{-h_{dmg} D} \tag{6}$$

The previous analysis found that the bond slip becomes significant on RC column responses to blast load when the bond shear modulus is less than 20 MPa/mm^2 and the maximum elastic slip is smaller than

Table 7
Parameters to define contact_1D.

bond shear modulus G_s (MPa)	maximum elastic slip u_{max} (mm)	damage curve exponent h_{dmg}
20	1.0	1.0

1.0 mm [53] while the influence of the exponential term is insignificant therefore can be neglected. In the present study, the shear modulus is assumed as 20 MPa/mm^2, the maximum elastic slip as 1.0 mm, and the exponential term is assumed to be 1.0.

In this model, the slave node of a string of beam or truss elements, modeling the rebar, is forced to slide along a master line of nodes embedded in the solid mesh, which models the concrete matrix. This kinematic constraint is applied using a penalty function approach. Fictitious springs are inserted between slave nodes and their projections over the master lines. These springs produce internal forces along the rebar and are proportional to the distance between slave nodes and master lines, as shown in Fig. 10.

Epoxy adhesive is applied to externally bond the FRP to the column. The influence of the adhesive to the strength and rigidity of the composite is usually negligible. It protects individual fibres while providing a mechanism for load-transfer and shear resistance. The Automatic_Surface_To_Surface_Tiebreak contact option in LS-DYNA is applied in this research to simulate the adhesive contact between the RC column and FRP. This special contact option depends on the variables of the tensile and shear failure stresses (*NFLS* and *SFLS*) of epoxy. These *NFLS* and *SFLS* values are based on the epoxy strength of Sikadur-30 for concrete-CFRP strip bond and Sikadur-330 for concrete-CFRP wrap bond. Failure of contact between CFRP composite and concrete surface occurs if

$$\left(\frac{|\sigma_n|}{NFLS}\right)^2 + \left(\frac{|\sigma_s|}{SFLS}\right)^2 \geqslant 1 \tag{7}$$

where σ_n and σ_s are the tensile and shear stresses at the interface, respectively. It is difficult to define the bond strength of this contact because their values vary from 4 MPa to 30 MPa [54] depending on the quality in applying the epoxy and CFRP, curing days and the temperature during the curing after application of CFRP. The adhesive properties of the FE models are defined according to the manufacturer Sika Kimia Pty. Ltd. and Syed-Ahmed research work that presented in Tables 8 and 9.

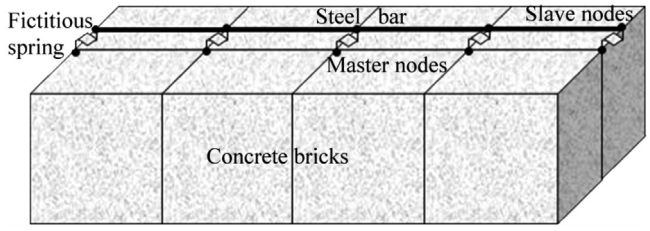

Fig. 10. Sketch of fictitious spring between master and slave nodes in one-dimensional slide line model.

Table 9
Epoxy adhesive properties by Syed-Ahmed.

Property	Value
Tensile Strength (*NFLS*)	32 MPa
Tensile Modulus	11.7 GPa
Shear Strength (*SFLS*)	29.4 MPa
Compressive Strength	60 MPa
Poisson's Ratio	0.2

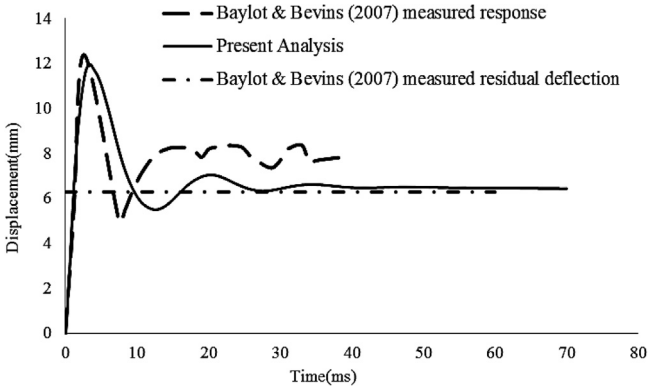

Fig. 11. Mid-height deflection time history [29].

4. Validation of finite element model

Fig. 11 shows the mid-height deflection time history in the experimental test and the numerical analysis. The maximum deflection is found to be close to the experimental value. The horizontal displacements of the middle height are 12.5 mm and 12 mm in the experiment and the present numerical analysis, respectively thereby indicating a difference of only approximately 4%. Residual deflections, however, are almost similar in both studies. The residual horizontal displacement of the mid-height of the column of 6.3 mm is obtained from the experiment. Therefore, we can conclude that by comparing the displacement and the maximum pressure, the simulation results match the experimental observation.

Fig. 12 is presented the maximum displacement measured in this study compare with the blast field test performed by Crawford et al. for loading case 2. The maximum displacement is measured for column retrofitted with FRP composite and without FRP. The maximum displacement for unstrengthened column in present study and experimental test are 46 mm and 48 mm respectively. While the maximum displacement for FRP strengthened column in present study and experimental test are 21 mm and 15 mm respectively. Comparing between the results obtained from the numerical results and blast test indicates the numerical results by the current FE model agree well with the experiment.

5. Baseline numerical model

In this research, the RC column is considered with dimensions of 500 mm × 700 mm and the height is set to 4400 mm. All longitudinal reinforcement bars have a circular cross-section with a diameter of

Table 8
Epoxy adhesive properties by manufacturer (Sika Kimia Pty. Ltd.).

Resin	Density (kg/m^3)	Tensile strength, (*NFLS*) (MPa)	Modulus of elasticity (GPa)	Elongation (%)	Shrinkage (%)
Epoxy	1.2–1.3	55–130	2.8–4.1	3.0–10.0	1–5

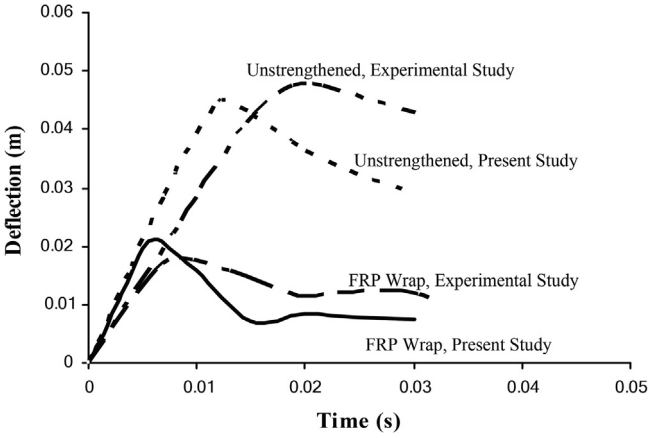

Fig. 12. Comparison of responses of FRP strengthened columns.

25 mm. The stirrups diameter is 12 mm with a spacing of 200 mm (see Fig. 13 for description). The mesh size of 50.0 mm is used for all element types. A pressure is applied on the top surface of the column via a ramp function to consider the static axial load before the blast simulation. The front face of the column is subjected to the explosive load. The material properties for studied columns are listed in Table 10 [31,45].

For retrofitted columns, three column blast strengthening techniques are conducted in the numerical models as presented in Fig. 14. They are columns retrofitted with FRP wrap, FRP strips and combined FRP strips and wrap. The thickness of FRP strips and FRP wrap are 3 and 5 mm respectively. In the columns with FRP strips, the wide of strips are 150 mm that three FRP strips are install in front and back side of the columns and two FRP strips are install in other side of the columns. Further investigation is also carried out to examine the change in FRP thickness and strength to columns retrofitted with FRP composites. The research compared the structural response of an un-retrofitted RC column with various column retrofitted with different FRP wrap thickness, strength and arrangement.

Adequate mesh size and appropriate element type are important in performing finite element analysis, especially for dynamic blast analysis. The main reason is because they are the key factors that ensure all frequencies generated from blast waves are captured by each of the elements. In this research, appropriate mesh size is determined by halving the size of mesh in finite element models. It indicates the mesh

Table 10
Properties of steel and concrete.

Material	Parameters	Value
Concrete	Uniaxial compressive strength	42 MPa
	Mass density	2400 kg/m^3
	Poisson's ratio	0.2
	Tensile stress at failure	6.0 MPa
Steel Reinforcement	Young's Modulus	200 GPa
	Yield stress	550 MPa
	Mass density	7800 kg/m^3
	Poisson's ratio	0.3
	Plastic strain at failure	0.12

size of 50 mm is suitable for analysis and further reduction in element size has insignificant effects on the results. Another reason to select the mesh size is computational cost. Therefore 50 mm mesh size is selected to reduce the computational cost. The element formulations used in this study are constant stress solid elements for the concrete and two-node Hughes–Liu beam elements for rebar [32,55]. To define the element formulation and integration rule, the Section_Solid keyword is used. In this research, the element formulation (ELFORM = 1) is defined in the numerical models. This option of formulation is known to be efficient, accurate and works on severe deformations. In addition, it requires less time in the analysis process. Boundary conditions are essential components for a successful analysis. Each analysis is uniquely defined for the evaluation of a specific geometry subjected to a specific set of loading and boundary environments. Boundary condition is one of the crucial factors in governing the behavior of the finite element model, especially in explosion analysis. In this case, the column is clamped in the heading and footing. Thus, we set the clamps in all the nodes of the heading and footing. To do this, we first set the list of the nodes in the tab SetD by selecting the nodes directly from the model Set Node. Then, in the tab SPC, we choose the degrees of freedom that we want to block. In this study, the bottom and top exterior nodes (see Fig. 15) are fixed except that top nodes are only free along Z-axis to withstand the axial load.

6. P–I diagram generation

Parametric simulation is performed here to understand the effect of material properties and dimensions of the RC column on the damage and dynamic response of the RC columns (see Table 11). Different simulations are performed based on a group of blast loads (see Table 12) to obtain different damage levels. The simulation results are used to

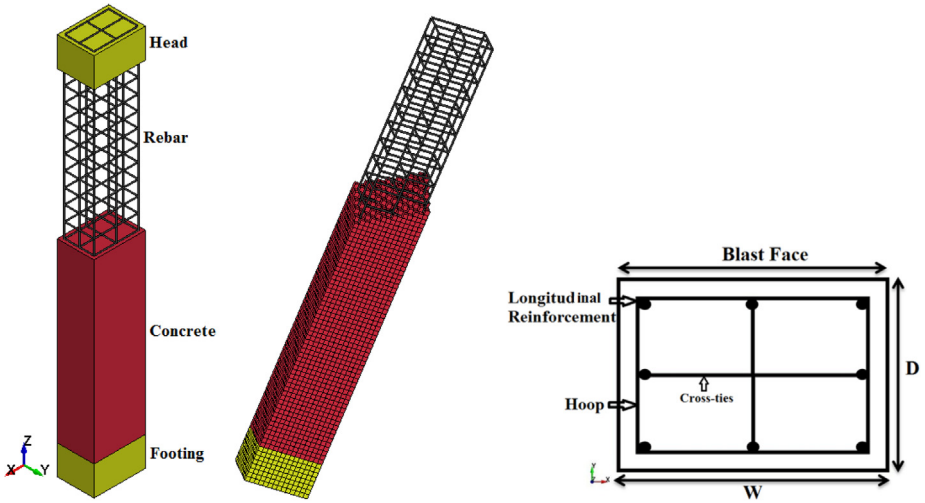

Fig. 13. Schematic view of the unstrengthened RC column.

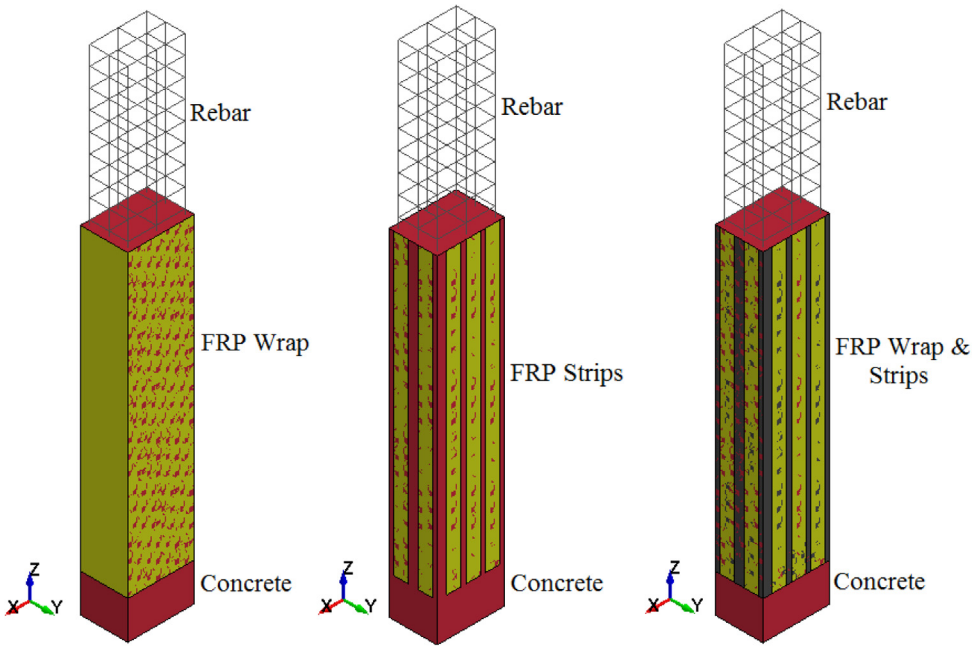

Fig. 14. FRP strengthened RC column configurations.

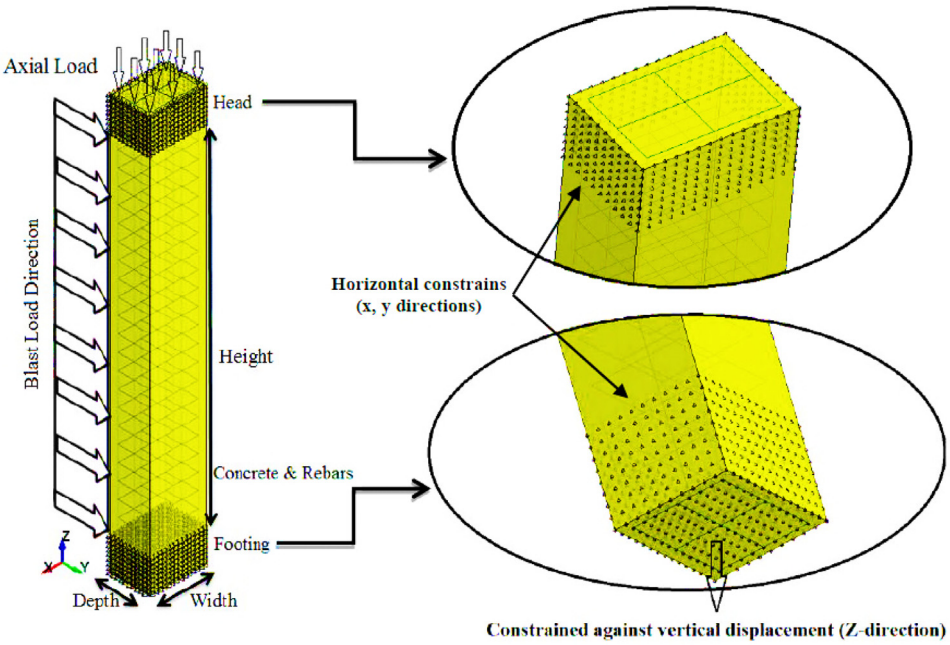

Fig. 15. Boundary condition of the simulated column.

Table 11
Summary of selected parameters and their limits.

Parameters	Symbols	Values	Units
Column depth	d	500,700,900	mm
Longitudinal reinforcement ratio	ρ	0.011,0.018,0.028	–
Transverse reinforcement ratio	ρ_s	0.0027,0.0048,0.0075	–
Concrete strength	f_c	32,42,52	MPa
Column height	H	3400,4400,5400	mm
Longitudinal steel strength	f_y	400,460,550	MPa
Transverse steel strength	f_{yt}	250,400,450	MPa
Column width	w	500,700,900	mm
Axial load index	ALI	0.1,0.2,0.3	–

evaluate the damage level. Then, the P-I diagram is constructed using the damage level. We determine the borderlines between the two damage levels using the curve-fit method. We construct P-I diagrams after finding all the boundary lines. The P–I diagram of three RC columns is shown in Fig. 16 (see Table 13 for the configuration). The damage degree (D) introduced in [22,23] is defined using Eq.8 and the corresponding equation for P_d is defined in Eq. (9).

$$D = 1 - \frac{P_r}{P_d} \tag{8}$$

$$P_d = 0.85 f_c (A_c - A_s) + f_y A_s \tag{9}$$

Table 12
Close in detonation magnitudes used in numerical analysis.

R(m)	M(kg)	Z(m/kg$^{1/3}$)
0.5	0.4	0.678604404
	0.6	0.592815551
	0.7	0.56312394
	0.73	0.555301761
	0.8	0.538608673
	0.9	0.538608673
	1.074	0.488242121
	1.1	0.484364653
	1.5	0.436790232
	1.917	0.403693854
	2	0.396850263
	3	0.346680637

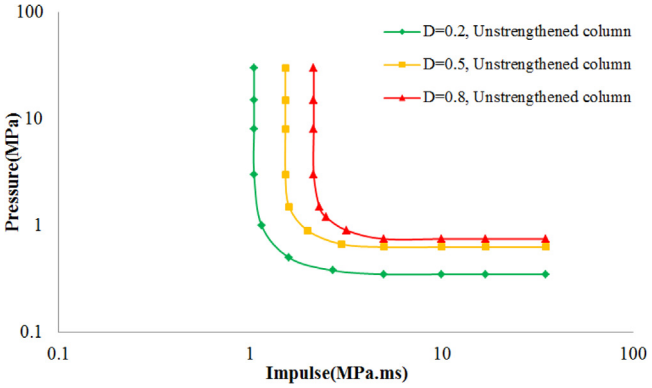

Fig. 16. P-I diagrams for unstrengthened RC column.

Where

P_d = the peak axial load carrying capacity of the intact column
P_r = the residual axial load carrying capacity of the damaged columns
A_S = cross-sectional areas of longitudinal reinforcements
A_c = cross-sectional areas of the column
f_y = the yield strength of the bars
f_c = the compressive strength of concrete

Meanwhile the FRP wrap develops a confinement pressure, the axial load resistance of undamaged column P_{rmax} for FRP retrofitted column is determined based on ISIS Canada as:

$$P_{r\max} = k_e\left[\beta_1\varphi_C f'_{CC}(A_C - A_S) + \varphi_S f_Y A_S\right]$$
$$\beta_1 = 0.85 - 0.0015f'_C \geqslant 0.67$$
$$f'_{CC} = f'_C(1 + \alpha_{PC}\omega_W)$$
$$\omega_W = \frac{2f_{frp}}{\varphi_C f'_C}$$

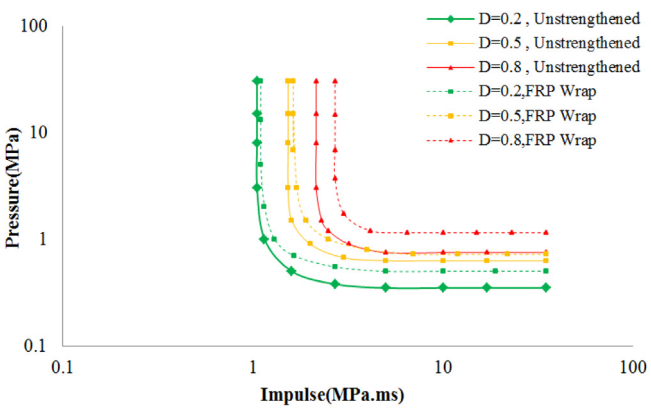

Fig. 17. P-I diagrams for RC column strengthened with FRP wrap.

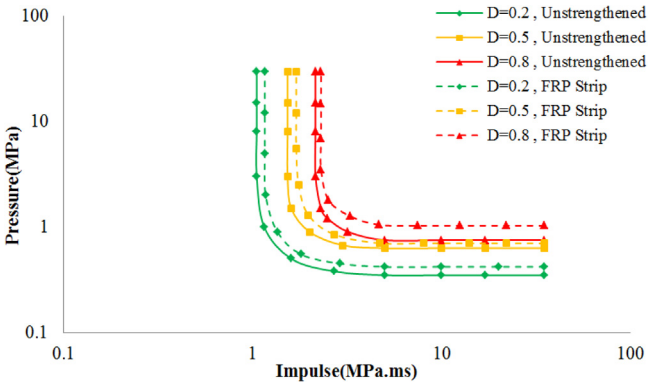

Fig. 18. P-I diagrams for columns strengthened with FRP strips.

where

k_e is a strength reduction factor applied for unexpected eccentricities (k_e = 0.85 for ductile column)
β_1 is ratio of average stress in rectangular compression block to the specified concrete compressive strength
Φ_C is resistance factor for concrete (Φ_C = 0.6)
Φ_S resistance factor for reinforcing bars (Φ_S = 0.85)
f'_{CC} is the compressive strength of the confined concrete
f_C is the unconfined compressive strength of the concrete
α_{PC} is the performance coefficient for a column and is suggested as 1.0
ω_w is a volumetric ratio of FRP strength to concrete strength
f_{frp} is the tensile strength of FRP

7. Results and discussion

The following sections describe the effects of various strengthening scheme on the pressure asymptote (P_0) and impulsive asymptote (I_0) of

Table 13
the configuration of the columns.

Column no.	Column width *(mm)*	Column depth *(mm)*	Column height *(mm)*	Cross tie/hoop	Longitudinal reinforcement
Un-strengthened RC Column	500	700	4400	Φ12@200	8Φ25

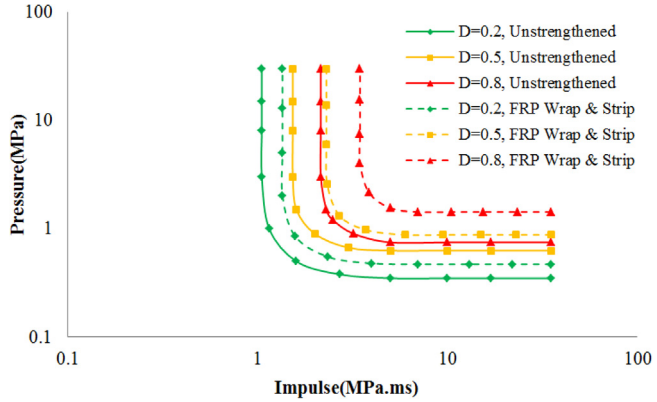

Fig. 19. P-I diagrams for columns retrofitted with FRP wrap and strips.

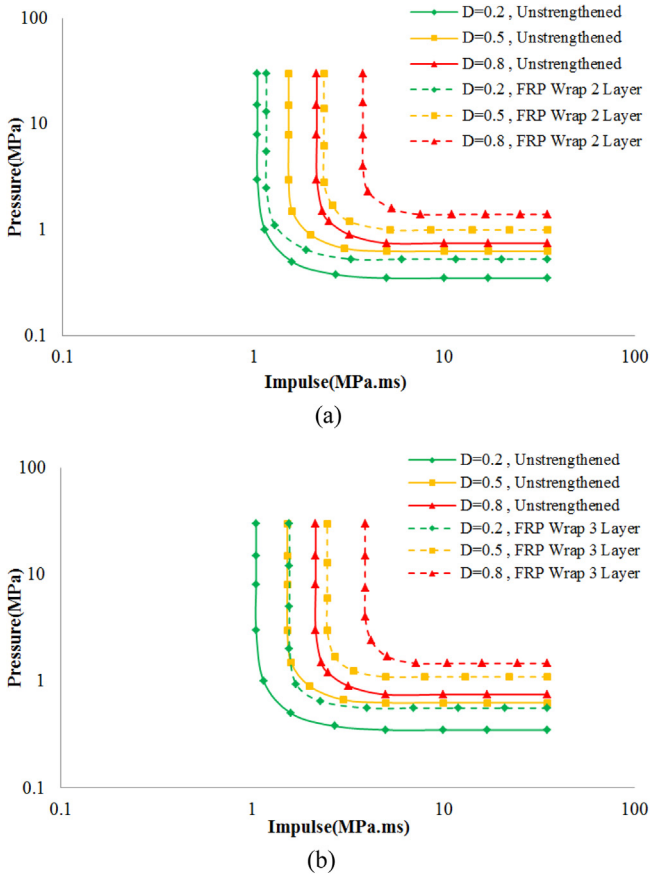

Fig. 20. P-I diagrams of columns retrofitted with (a) 2 layers and (b) 3 layers of FRP wrap.

the RC columns. Strengthening scheme are FRP wrap, FRP strips, combined FRP wrap & strips, FRP wrap with different layer, different FRP strength, and various FRP thickness.

7.1. The influence of FRP wrap

Intensive numerical simulations are conducted with the above finite element models to evaluate the influences of FRP wrap on the P-I curves of FRP retrofitted column exposed to blast detonation. The strength of FRP wrap in the analysis is 2280 MPa. Other parameters of the columns are $w = 700$ mm, $d = 500$ mm, H = 4400 mm, $f_c = 42$ MPa, $f_y = 460$ MPa, $\rho = 0.011$, $\rho_s = 0.0027$. Fig. 17 presents the P-I diagrams of columns retrofitted with FRP wraps. Also, the corresponding P-I curves of the un-retrofitted column are also shown in the figure for comparison. As can be seen from Fig. 17, both the P_0 and I_0 of the column strengthened with FRP wraps increased. It can be observed that RC columns strengthened with FRP wraps increased column resistance to failure under explosive loads.

7.2. The influence of FRP strips

In this section, P-I curves of columns retrofitted with FRP strips are presented. In this study, the FRP strips thickness is 3 mm and the FRP strength is 2280 MPa. Other parameters of the columns are $w = 700$ mm, $d = 500$ mm, H = 4400 mm, $f_c = 42$ MPa, $f_y = 460$ MPa, $\rho = 0.011$, $\rho_s = 0.0027$. Fig. 18 present the P-I curve of columns retrofitted with FRP strips and unstrengthened column under blast load condition. The results reveal that although severe damage can still be seen for locations in close proximity to the explosive charge, the use of FRP strips did reduce the dynamic response of the RC columns as compared to the unprotected case scenario. As can be seen from Fig. 18, both the P_0 and I_0 of the column retrofitted with FRP strips increased. It can be observed that columns retrofitted with FRP strips increased column resistance to failure under explosive loads.

Table 14
Three different material properties of FRP composite.

Mechanical Properties	Han et al. (2007) Carbon/epoxy braid	Soden et al. (1998) Carbon/epoxy (AS4/3501–6)	Chan et al. (2007) Carbon/epoxy (AS4/3501–6)
Density (kg/m^3), ρ	1795	1580	1580
Longitudinal modulus (GPa), E_1	118	126	138
Transverse modulus (GPa), E_2	5.5	11	9.65
In-plane shear modulus, G_{21}	4.8	6.6	5.24
Out-of-plane shear modulus, G_{23}	4.8	6.6	2.24
Minor Poisson's ratio, ν_{21}	0.1172	0.024	0.021
Through thickness Poisson' ratio, ν_{31}	0.1172	0.024	0.021
Longitudinal tensile strength (MPa), X_T	**1095**	**1950**	**2280**
Longitudinal compressive strength (MPa), X_C	712.9	1480	1440
Transverse tensile strength (MPa), Y_T	26.4	48	57
Transverse compressive strength (MPa), Y_C	84.4	200	228
In-plane shear strength (MPa), S	84.3	79	71
Maximum strain for fibre tension (%), ε_t	2.3	1.38	1.38
Maximum strain for fibre compression (%), ε_c	1.4	1.175	1.175

7.3. The influence of FRP wrap & strips

To evaluate the P-I diagram of FRP wrap and strips on the column, reactions of columns retrofitted with 5 mm FRP wrap thickness and 3 mm FRP strip thickness are evaluated. The strength of FRP wrap in the analysis is 2280 MPa. Other parameters of the columns are w = 700 mm, d = 500 mm, H = 4400 mm, f_c = 42 MPa, f_y = 460 MPa, ρ = 0.011, ρ_s = 0.0027. The comparisons of the pressure asymptote and impulsive asymptote of columns with and without FRP strengthening are displayed in Fig. 19. It is observed that using the FRP wrap and strips is significant in increasing the blast load resistance capacity of columns. The outcomes indicate that the explosion resistance of column without FRP is significantly less than that of a column with FRP strengthening. The columns retrofitted with combined FRP wrap and strips have the highest blast resistance capacity compared with columns retrofitted with separate FRP wrap and strips.

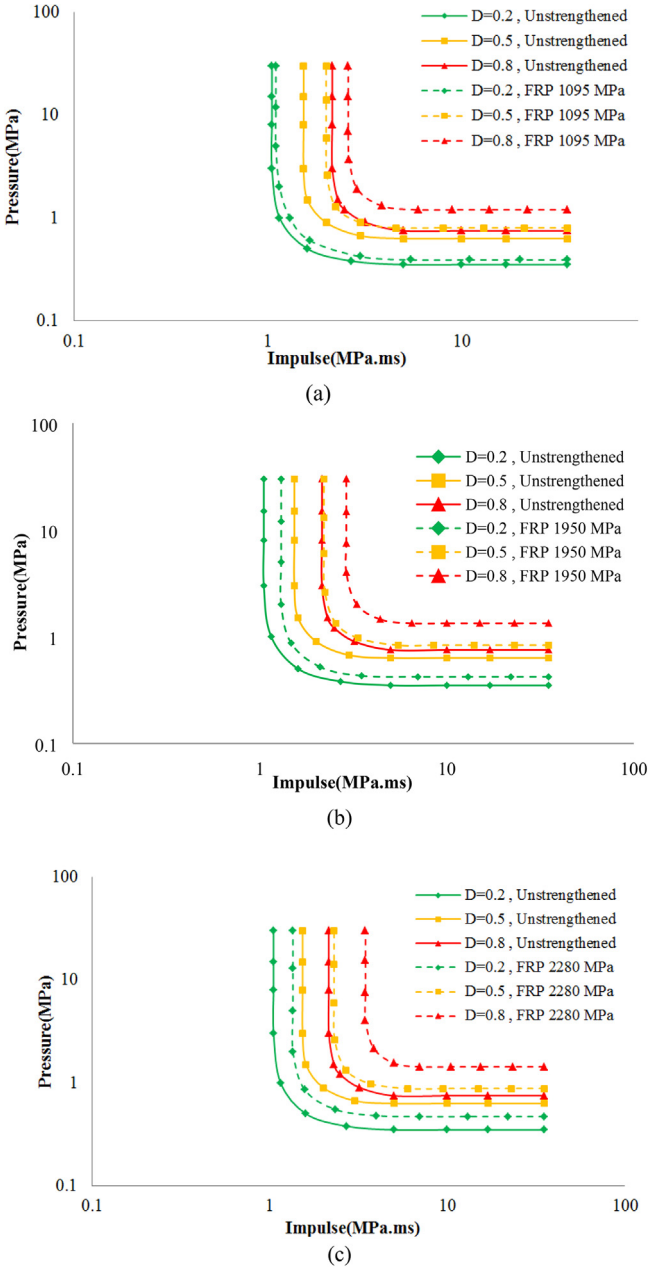

Fig. 21. P-I diagrams of FRP retrofitted column with FRP strength of (a) 1095 MPa, (b) 1950 MPa and (c) 2280 MPa.

7.4. The influence of FRP wrap with different layer

To study the P-I diagram for different FRP wrap layers on the columns, behaviour of columns retrofitted with 5 mm FRP wrap thickness is calculated. The strength of FRP wrap in the analysis is 2280 MPa. Other parameters of the columns are w = 700 mm, d = 500 mm, H = 4400 mm, f_c = 42 MPa, f_y = 460 MPa, ρ = 0.011, ρ_s = 0.0027. Fig. 20 shows the effect of using more layer of FRP wrap on the P-I curve of the blast-damaged columns. The results show that using more layers of FRP wrap considerably increases the column explosion resistance capacity. Therefore, columns with more FRP layers would suffer less damage from blast loads. As a result, the P–I curve translates to the right. In this case, impulse asymptotes rise more than pressure asymptotes.

7.5. The influence of FRP strength on P-I diagram

Intensive numerical models are developed to study effects of various FRP material strengths on P_0 and I_0 of the RC columns. To study the P-I diagram for different FRP material strengths on the columns, behaviour of columns retrofitted with 5 mm FRP wrap thickness and 3 mm FRP strips thickness is demonstrated. Three distinct FRP material strength parameters are used namely 1095, 1950 and 2280 MPa. The properties of FRP material strengths are presented in Table 14 [46,56,57]. The parameters of the columns are w = 700 mm, d = 500 mm, H = 4400 mm, f_c = 42 MPa, f_y = 460 MPa, ρ = 0.011, ρ_s = 0.0027. Fig. 21 presented P-I diagrams of FRP retrofitted column with FRP strength of (a) 1095 MPa, (b) 1950 MPa and (c) 2280 MPa. Generally, columns with increased FRP material

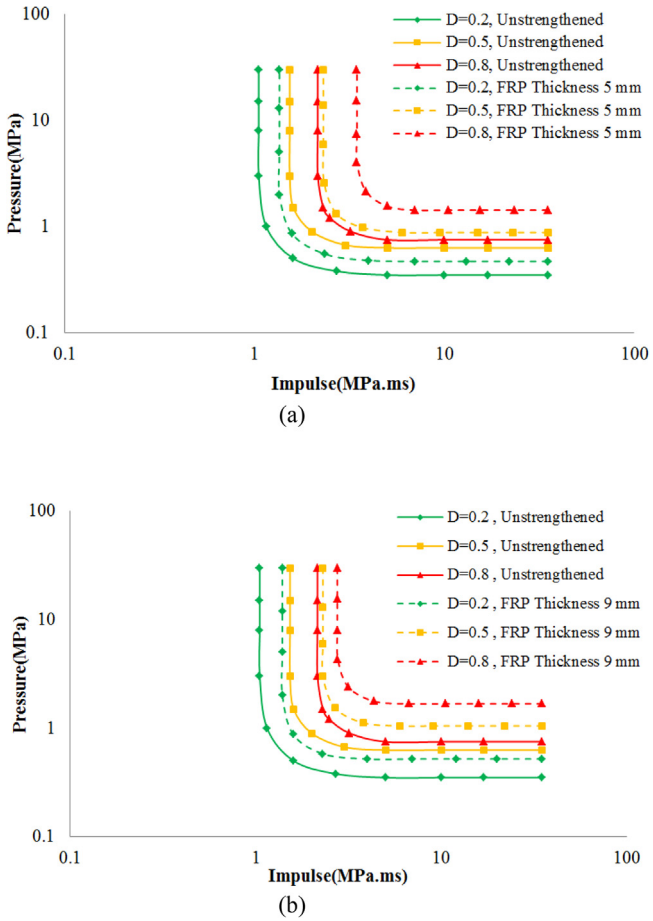

Fig. 22. The influence of FRP wrap thickness on the P-I diagram with (a) 5 mm thickness and (b) 9 mm thickness.

strengths have higher explosion capacity. Therefore, P–I curve moves toward the right, leading to less damage with the same blast loads. The results indicate FRP material strength has a significant effect on P-I diagram of the retrofitted column.

7.6. The influence of FRP thickness on P-I diagram

Pressure impulse curves are developed for FRP retrofitted columns with various FRP wrap thicknesses. In this study, the FRP wrap thicknesses are 3, 5 and 9 mm. The strength of FRP wrap in the analysis is 2280 MPa. Other parameters of the columns are w = 700 mm, d = 500 mm, H = 4400 mm, f_c = 42 MPa, f_y = 460 MPa, ρ = 0.011, ρ_s = 0.0027. Simulated P–I curve for columns with various FRP wrap thickness is displayed in Fig. 22. The results demonstrated that as the FRP wrap thickness increases, the impulsive and pressure asymptotes of the P–I curve increased. Consequently, the P–I curve shifts toward the right. This shift represents less considerable damage under the same blast.

The above results demonstrated the effectiveness of FRP strengthening on RC column blast loading resistance capacities. The results indicate that the FRP strength, thickness and configurations all affect the strengthening effectiveness. In general, strengthening the column with FRP wrap is more effective than FRP strip because the FRP wrap not only provides extra strength, but also confinement to the concrete, which will increase the RC column strength.

8. Analytical formulae to generate P–I diagram

As shown, the P-I curves for FRP strengthened column can also be represented by hyperbolic equations. Similar observations are also made in [58,59]. Consequently, equations are applied to indicate the P-I curves of FRP retrofitted column. Hence the P-I diagram formula can be expressed as

$$(P - P_0)(I - I_0) = 3\left(\frac{P_0}{2} + \frac{I_0}{2}\right)^{1.5} \tag{11}$$

Comparison between numerical simulation results with Eq. (11) for non-retrofitted column and FRP retrofitted columns with wrap and strips are presented in Figs. 23 and 24. The dashed lines indicate the P-I curves generated by the equation (6) and the solid lines represent the P-I diagrams generated by numerical analysis data. As shown, the hyperbolic equation closely matches the simulated P-I diagrams.

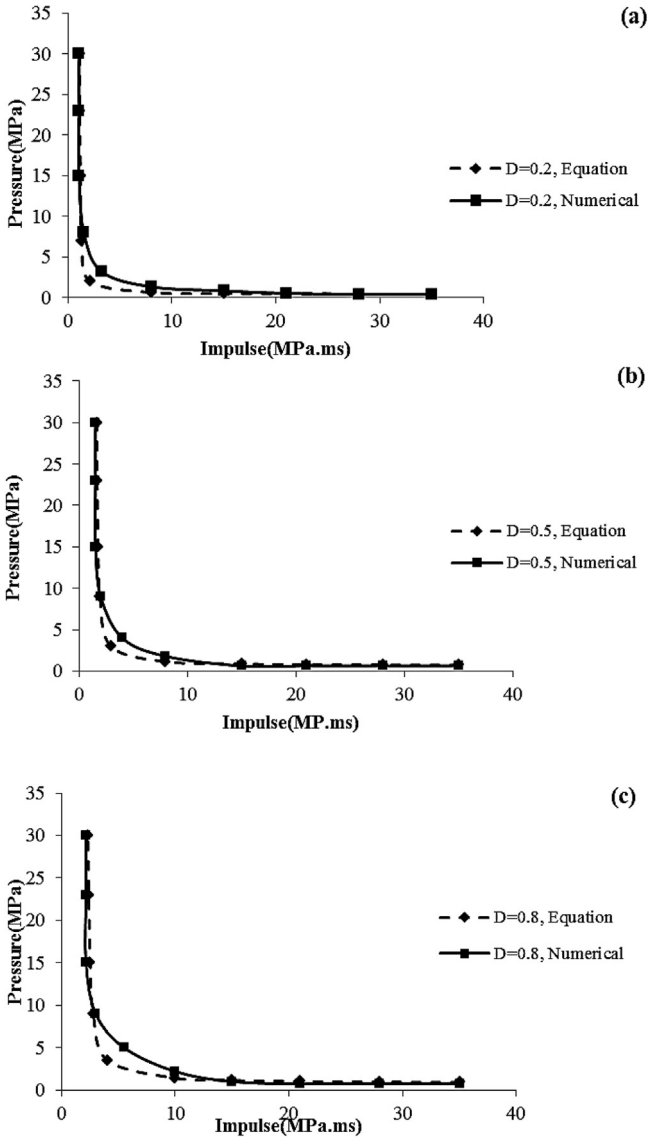

Fig. 23. Derivation of P-I diagrams using Eq. (11) and FE models (non-retrofitted columns).

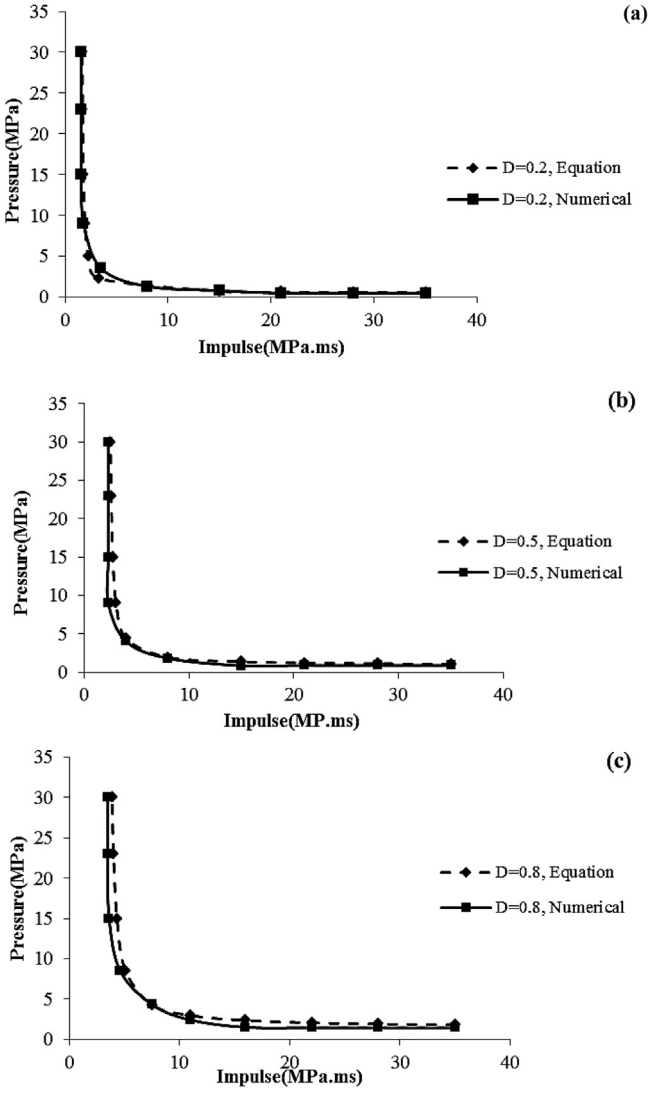

Fig. 24. Derivation of P-I diagrams using Eq. (11) and FE models (FRP retrofitted columns).

9. Conclusion

In this research, various methods of material strengthening against high-amplitude, short-duration blast loads are investigated by running computer simulations using the commercial software LS-DYNA. This research also addresses methods for applying explosive blast loads to finite element models. Additionally, the research uses the findings from the investigations to construct P-I diagram for un-retrofitted and FRP retrofitted columns. Additionally, the research serves to provide a validation for using the finite element model for testing un-retrofitted and FRP retrofitted RC columns by comparing the simulation models to similar blast field tests. Further investigation is also carried out to generate pressure and impulse asymptotes of columns by change in FRP strengthening scheme. The results showed that FRP successfully strengthens RC columns against blast loading. Based on the results, strengthening with FRP is an effective way of increasing the flexural capacity and stiffness to resist high strain rate events of columns exposed to blast loads. The generated P–I curve models can be applied by engineers to predict damage levels of new columns and to assess existing columns subjected to various blast load conditions.

CRediT authorship contribution statement

M. Abedini: Conceptualization, Methodology, Software, Validation, Data curation, Writing - original draft. **Chunwei Zhang:** Supervision, Project administration, Funding acquisition.

Declaration of Competing Interest

The authors declare that they have no known competing financial interests or personal relationships that could have appeared to influence the work reported in this paper.

Acknowledgement

This research is financially supported by the Ministry of Science and Technology of China (Grant No. 2019YFE0112400), the Key Research and Development Program of Liaoning Province (Grant No. 2017231010), the Taishan Scholar Priority Discipline Talent Group program funded by the Shandong Province, and the first-class discipline project funded by the Education Department of Shandong Province.

References

[1] Zhang C, Gholipour G, Mousavi AA. Nonlinear dynamic behavior of simply-supported RC beams subjected to combined impact-blast loading. Eng Struct 2019;181:124–42.
[2] UFC-3-340-02, Design of structures to resist the effects of accidental explosions, ed. US Army Corps of Engineers, Naval Facilities Engineering Command Air Force Civil Engineer Support Agency, Dept of the Army and Defense Special Weapons Agency 2008 Washington DC
[3] ASCE, Blast protection of buildings, in: American Society of Civil Engineers (ASCE), ed. Reston, VA, USA.: ASCE-59-11, 2011
[4] TM5-1300, Structures to resist the effects of the accidental explosions, in: Technical Manual ed: US Department of Army, Picatinny Arsenal, New Jersey, 1990.
[5] Xu J, Wu C, Xiang H, Su Yu, Li Z-X, Fang Q, et al. Behaviour of ultra high performance fibre reinforced concrete columns subjected to blast loading. Eng Struct 2016;118:97–107.
[6] Zhang F, Wu C, Zhao X-L, Heidarpour A, Li Z. Experimental and numerical study of blast resistance of square CFDST columns with steel-fibre reinforced concrete. Eng Struct 2017;149:50–63.
[7] Shin J, Jeon J-S. Retrofit scheme of FRP jacketing system for blast damage mitigation of non-ductile RC building frames. Compos Struct 2019;228:111328.
[8] Abedini M, Mutalib AA. Investigation into damage criterion and failure modes of RC structures when subjected to extreme dynamic loads. Arch Computat Methods Eng 2020;27(2):501–15.
[9] Gholipour G, Zhang C, Mousavi AA. Nonlinear numerical analysis and progressive damage assessment of a cable-stayed bridge pier subjected to ship collision. Mar Struct 2020;69:102662.
[10] Liu S, Zhou Y, Zhou J, Zhang B, Jin F, Zheng Q, et al. Blast responses of concrete beams reinforced with GFRP bars: Experimental research and equivalent static analysis. Compos Struct 2019;226:111271.
[11] Liu L, Zong Z, Gao C, Yuan S, Lou F. Experimental and numerical study of CFRP protective RC piers under contact explosion. Compos Struct 2020;234:111658.
[12] Maazoun A, Belkassem B, Reymen B, Matthys S, Vantomme J, Lecompte D. Blast response of RC slabs with externally bonded reinforcement: Experimental and analytical verification. Compos Struct 2018;200:246–57.
[13] Merrifield R. Simplified calculations of blast induced injuries and damage: Health and Safety Executive. Technol Health Sci Div 1993.
[14] Smith PD, Hetherington JG. Blast and ballistic loading of structures. London: Butterworth Heinemann; 1994.
[15] Thiagarajan G, Rahimzadeh R, Kundu A. Study of pressure-impulse diagrams for reinforced concrete columns using finite element analysis. Int J Protect Struct 2013;4(4):485–504.
[16] Syed ZI, Liew MS, Hasan MH, Venkatesan S. Single-degree-of-freedom based pressure-impulse diagrams for blast damage assessment. Appl Mech Mater 2014;567:499–504.
[17] Hamra L, Demonceau J-F, Denoël V. Pressure–impulse diagram of a beam developing non-linear membrane action under blast loading. Int J Impact Eng 2015;86:188–205.
[18] Dragos J, Wu C, Haskett M, Oehlers D. Derivation of normalized pressure impulse curves for flexural ultra high performance concrete slabs. J Struct Eng 2013;139(6):875–85.
[19] Fallah A, Nwankwo E, Louca L. Pressure-impulse diagrams for blast loaded continuous beams based on dimensional analysis. J Appl Mech 2013;80. https://doi.org/10.1115/1.4023639.
[20] Colombo M, Martinelli P. Pressure–impulse diagrams for RC and FRC circular plates under blast loads. Eur J Environ Civil Eng 2012;16(7):837–62.
[21] Abedini M, Mutalib AA, Raman SN, Alipour R, Akhlaghi E. Pressure–impulse (P–I) diagrams for reinforced concrete (RC) structures: a review. Arch Computat Methods Eng 2019;26(3):733–67.
[22] Shi Y, Hao H, Li Z-X. Numerical derivation of pressure–impulse diagrams for prediction of RC column damage to blast loads. Int J Impact Eng 2008;35:1213–27.
[23] Mutalib AA, Hao H. Development of P-I diagrams for FRP strengthened RC columns. Int J Impact Eng 2011;38(5):290–304.
[24] Li QM, Meng H. Pressure-impulse diagram for blast loads based on dimensional analysis and single-degree-of-freedom model. J Eng Mech 2002;128(1):87–92.
[25] Mays GC, Smith PD. Blast effects on buildings; Design of buildings to optimize resistance to blast loading. London, UK: Thomas Telford; 1995.
[26] Liu F, Deng S, Zhang J. Mechanical properties of epoxy and its carbon fiber composites modified by nanoparticles. J Nanomater 2017;2017:1–9.
[27] Matykiewicz D. Hybrid epoxy composites with both powder and fiber filler: A review of mechanical and thermomechanical properties. Materials 2020;13:1802.
[28] Rahmani H, Najafi SHM, Saffarzadeh-Matin S, Ashori A. Mechanical properties of carbon fiber/epoxy composites: Effects of number of plies, fiber contents, and angle-ply layers. Polym Eng Sci 2014;54:2676–82.
[29] Baylot JT, Bevins TL. Effect of responding and failing structural components on the airblast pressures and loads on and inside of the structure. Comput Struct 2007;85(11-14):891–910.
[30] Crawford JE, Malvar LJ, Wesevich JW, Valancius J, Reynolds AD. Retrofit of reinforced concrete structures to resist blast effects. Am Concr Inst Struct J 1997;94:371–7.
[31] Abedini M, Zhang C, Mehrmashhadi J, Akhlaghi E. Comparison of ALE, LBE and pressure time history methods to evaluate extreme loading effects in RC column. Structures 2020:456–66.
[32] LS-DYNA, "Keyword User's Manual V971,CA: Livermore Software Technology Corporation(LSTC),Livermore, California," ed, 2015.
[33] Zhang C, Mousavi AA. Blast loads induced responses of RC structural members: State-of-the-art review. Compos B Eng 2020:108066.
[34] Abedini M, Mutalib AA, Zhang C, Mehrmashhadi J, Raman SN, Alipour R, Momeni T, Mussa MH. Large deflection behavior effect in reinforced concrete columns exposed to extreme dynamic loads. Front Struct Civ Eng 2020;14(2):532–53.
[35] Abedini M, Zhang C. Performance assessment of concrete and steel material models in LS-DYNA for enhanced numerical simulation, a state of the art review. Archiv Comput Methods Eng 2020:1–22.
[36] Bao X, Li B. Residual strength of blast damaged reinforced concrete columns. Int J Impact Eng 2010;37(3):295–308.
[37] Mutalib AA, Hao H. Numerical analysis of FRP-composite-strengthened RC panels with anchorages against blast loads. J Perform Constr Facil 2011;25(5):360–72.
[38] Mutalib AA, Tawil NM, Baharom S, Abedini M. Failure probabilities of FRP strengthened RC column to blast loads. Jurnal Teknologi 2013;65.
[39] Yonten K. An evaluation of constitutive models of concrete in LS-DYNA finite element code. 15th ASCE Engineering Mechanics Conference Columbia University, 2002.
[40] Thabet A, Haldane D. Three-dimensional simulation of nonlinear response of reinforced concrete members subjected to impact loading. ACI Struct J 2000;97:689–702.
[41] William KJ, Warnke EP. Constitutive Models for the Triaxial Behavior of Concrete. In: Concrete structures subjected to triaxial stresses, International Association of Bridge Structural Engineering Proceedings, Bergamo, Italy. p. 1–30.
[42] Malvar LJ, Morrill KB, Crawford JE. Numerical Modeling of Concrete Confined by Fiber-Reinforced Composites. J Compos Constr 2004;8(4):315–22.
[43] L. E. Schwer and L. J. Malvar, "Simplified concrete modeling with* MAT_CONCRETE_DAMAGE_REL3," JRI LS-Dyna User Week, pp. 49-60, 2005.
[44] Zhang C, Abedini M, Mehrmashhadi J. Development of pressure-impulse models and residual capacity assessment of RC columns using high fidelity Arbitrary Lagrangian-Eulerian simulation. Eng Struct 2020;224:111219.

[45] Chan S, Fawaz Z, Behdinan K, Amid R. Ballistic limit prediction using a numerical model with progressive damage capability. Compos Struct 2007;77(4):466–74.
[46] Wu J, Liu X, Zhou H, Li L, Liu Z. Experimental and numerical study on soft-hard-soft (SHS) cement based composite system under multiple impact loads. Mater Des 2018;139:234–57.
[47] Nam J-W, Kim H-J, Kim S-B, Yi N-H, Kim J-H-J. Numerical evaluation of the retrofit effectiveness for GFRP retrofitted concrete slab subjected to blast pressure. Compos Struct 2010;92:1212–22.
[48] Glanville WH, Grime G, Fox EN, Davies WW. An investigation of the stresses in reinforced concrete piles during driving. HM Stationery Office; 1938.
[49] C. e.-i. d. béton, CEB-FIP model code 1990: design code: Telford,V(213-214), https://doi.org/10.1680/ceb-fipmc1990.35430.fm, 1993.
[50] Marsh KJ, Campbell JD. The effect of strain rate on the post-yield flow of mild steel. J Mech Phys Solids 1963;11(1):49–63.
[51] Malvar LJ. Review of static and dynamic properties of steel reinforcing bars. ACI Mater J 1998;95.
[52] Shi Y, Li ZX, Hao H. Bond slip modelling and its effects on numerical analysis of blast-induced responses of RC columns. Struct Eng Mech 2009;32:251–67.
[53] Sika-Australia-Pty-Ltd. Structural Strengthening. Available: http://www.sika.com.au/cmc/Structural_Strengthening.htm
[54] J. O. Hallquist, “LS-DYNA theory manual,” vol. 3, ed: Livermore software Technology corporation, 2006.
[55] Soden P, Hinton M, Kaddour A. Lamina properties, lay-up configurations and loading conditions for a range of fibre-reinforced composite laminates. Compos Sci Technol 1998;58:1011–22.
[56] Han H, Taheri F, Pegg N, Lu Y. A numerical study on the axial crushing response of hybrid pultruded and ±45° braided tubes. Compos Struct 2007;80(2):253–64.
[57] FACEDAP, “Facility and component explosive damage asessment program,” SwRI Project No.06-5145-001, U.S. Army Corps of Engineers, Omaha District, Omaha., vol. U.S. Army Corps of Engineers, Omaha District, Omaha., 1994
[58] Shi Y, Hao H, Li ZX. Numerical derivation of pressure-impulse diagrams for prediction of RC column damage to blast loads. Int J Impact Eng 2007;32:251–67.
[59] Shope RL. Comparisons of an alternative pressure-impulse (P-I) formulation with experimental and finite element results. The International Symposium on the Effects of Munitions with Structures (ISIEMS) 12.1, 2007.